Acta Mechanica Solida Sinica, Vol. 28, No. 3, June, 2015 ISSN 0894-9166
Published by AMSS Press, Wuhan, China

DETERMINATION OF FRACTURE TOUGHNESS OF BRITTLE MATERIALS BY INDENTATION**

Yihui Feng[1] **Taihua Zhang**[2*]

([1] *State Key Laboratory of Nonlinear Mechanics, Institute of Mechanics, Chinese Academy of Sciences, Beijing* 100190*, China*)

([2] *College of Mechanical Engineering, Zhejiang University of Technology, Hangzhou* 310014*, China*)

Received 20 March 2014, revision received 2 December 2014

ABSTRACT Fracture toughness is one of the crucial mechanical properties of brittle materials such as glasses and ceramics which demonstrate catastrophic failure modes. Conventional standardized testing methods adopted for fracture toughness determination require large specimens to satisfy the plane strain condition. As for small specimens, indentation is a popular, sometimes exclusive testing mode to determine fracture toughness for it can be performed on a small flat area of the specimen surface. This review focuses on the development of indentation fracture theories and the representative testing methods. Cracking pattern dependent on indenter geometry and material property plays an important role in modeling, and is the main reason for the diversity of indentation fracture theories and testing methods. Along with the simplicity of specimen requirement is the complexity of modeling and analysis which accounts for the semi-empirical features of indentation fracture tests. Some unresolved issues shaping the gap between indentation fracture tests and standardization are also discussed.

KEY WORDS indentation, fracture toughness, indenter geometry, cracking patterns

I. INTRODUCTION

Since Palmqvist[1–3] initially exhibited the potential significance of indentation-induced cracking to characterize the toughness of brittle materials, indentation fracture testing (IFT) in determining the fracture toughness (K_{IC}) of brittle materials on small scales has been the research hotspot over the past half century. Due to the requirements of sample size and shape in conventional fracture testing (CFT), there are few choices other than IFT when the test sample is small. On the other hand, due to the complication of contact/fracture problems, there is still no single model or method which can be applied to most brittle materials. Each existing method assumes a specific cracking pattern and is appropriate for a certain category of materials.

Several informative reviews on IFT have been published in 1980s and 1990s. Cook and Pharr[4] delivered a comprehensive review on the experimental investigations on Vickers IFT. Ostojic and McPherson[5] reviewed the basic principles of indentation fracture. Ponton and Rawlings[6,7] made an experimental investigation to assess the validity of some representative Vickers IFT methods. A great progress in the research on indentation fracture has been made in the past twenty years. New phenomena have been observed and new testing methods have been developed. Three-sided Berkovich and cube-corner indenters other than four-sided Vickers indenters have also become important options

* Corresponding author. E-mail: zhangth@zjut.edu.cn

** Project supported by the National Natural Science Foundation of China (Nos. 11302231, 11025212 and 11272318).

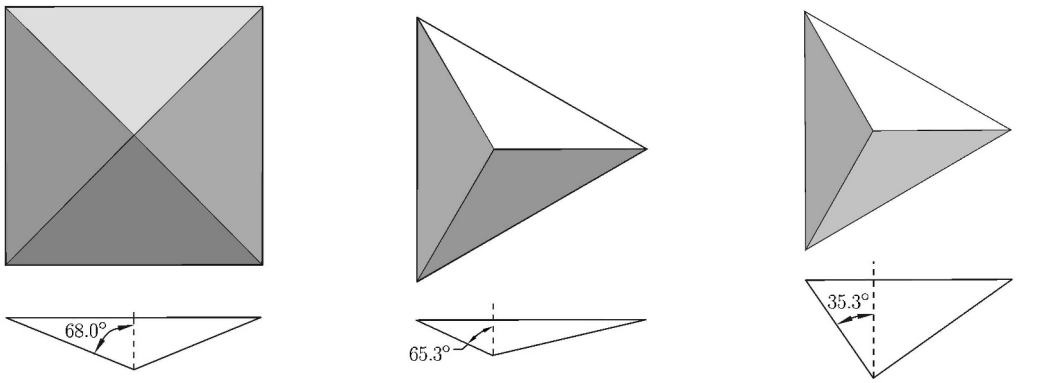

(a) Vickers, four-sided, with a face-to-axis angle of 68.0°

(b) Berkovich, three-sided, with a face-to-axis angle of 65.3° and the same depth-projected area relation as Vickers

(c) Cube-corner, three-sided, with a face-to-axis angle of 35.3°

Fig. 1. Three typical pyramidal indenters for indentation fracture testing.

for certain testing conditions. By virtue of the development of electromechanical techniques, machines with the function of instrumented indentation testing (IIT) have prevailed in IFT. Compared with Vickers hardness tester usually adopted in classic IFT, IIT machines have additional functions other than producing cracks, such as measuring elastic modulus and indentation works. Consequently some IIT-aided IFT methods have been developed in recent years. Thus there is a need to make a review to cover these improvements.

This review focuses on IFT methods and related theories for bulk brittle materials although there is also a strong demand of measuring the fracture toughness of hard coatings as well. Due to the complication of coating/substrate system, IFT methods for hard coatings were generally developed based on the combination of fracture energy concept and simplified cracking patterns. Chen et al.[8] recently made an informative review on IFT methods for hard coatings[9] which may give a bird's-eye view of this aspect to the interested.

II. INDENTATION CRACKING PATTERNS

Knowledge on the geometric features of crack faces underlies the modeling of indentation fracture, and determines how crack size plays its role in an IFT method. Thus it is crucial to be aware of the cracking patterns and its evolving process before establishing or using an IFT method.

Three kinds of pyramidal indenters (see Fig.1) and spherical indenters with different radii are usually used in IFT. Indentation-induced cracking patterns are dependent mainly on the geometry of the indenter[4, 10–12] and secondarily on the material properties of the sample[4, 13]. As for a pyramidal indenter, the cracking pattern in the indented brittle specimen generally includes one or several of the following separate crack types, (i) median crack (see Fig.2(a)), which resides below the indentation site, initiates at the elastic/plastic boundary, extends upward and downward and finally forms into a penny-like crack face; (ii) radial crack (see Fig.2(b)), which resides near the sample surface and emanates radially from the indentation corner; (iii) lateral crack (see Fig.2(c)), which resides blow the indentation site and extends nearly parallel to the sample surface. In many cases with Vickers indenter, the median and radial cracks coalesce into half-penny cracks (see Fig.2(d)). As for a spherical indenter, it usually produces in the brittle specimen a truncated cone crack face (see Fig.2(e)) which forms a ring crack trace at the sample surface. The property of indented materials has effect on some important details of cracking pattern such as the relative length of radial crack for pyramidal indentations and the angle of cone crack for spherical indentations.

The evolving process of cracking patterns during the loading-unloading cycle of indentation is critical to the rationality of indentation fracture analysis and the validity of IFT methods. As for pyramidal indentations, according to stress field analyses and experimental observations[4, 14–16], median cracks usually initiate and extend during the loading phase, radial cracks initiate in the late loading phase or the early unloading phase and extend forward during the unloading phase (see Fig.3), the lateral

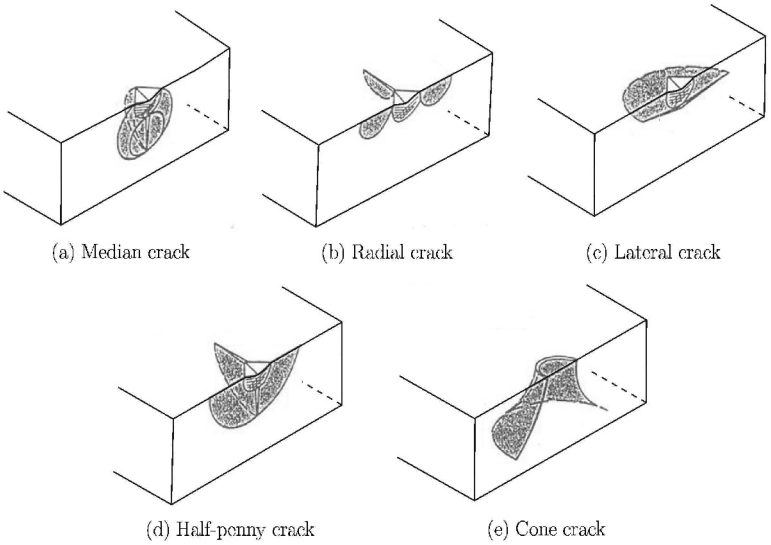

Fig. 2. Typical cracking patterns in indentation fracture tests[4].

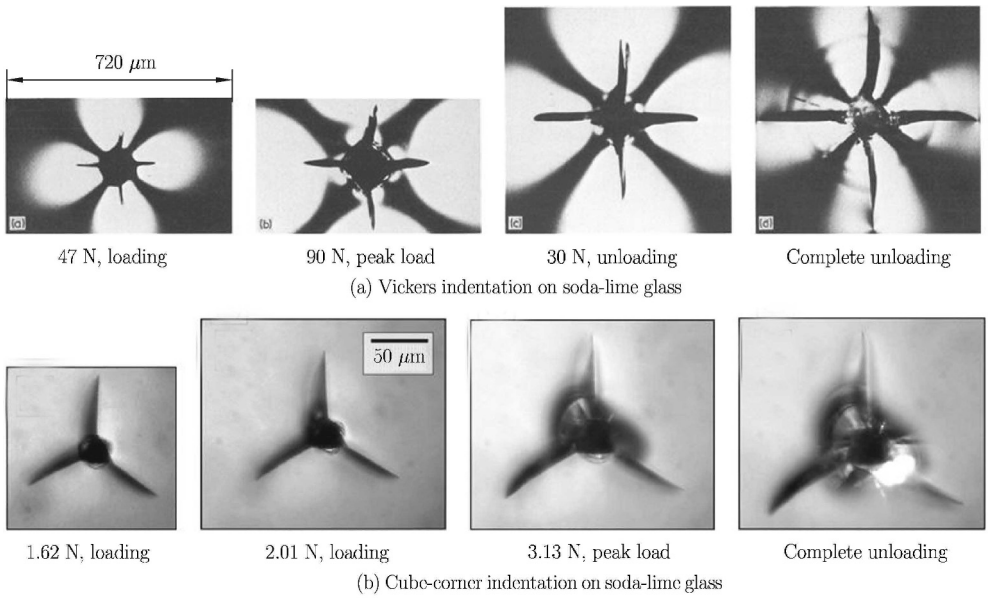

Fig. 3. The initiation and propagation process of pyramidal-indentation-induced radial cracks during the indentation cycle[15, 16].

cracks usually initiate and extend at the end of unloading process. The enhancing feature of radial cracks in the unloading phase justifies most existing IFT methods using pyramidal indenters. As for spherical indentations, according to stress analyses and experimental observations[17–21], a superficial ring crack perpendicular to the specimen surface initiates outside the edge of contact area when the indentation load reaches a threshold value. Increasing the indentation load will make the ring crack extend downward at a certain angle and finally form into a truncated cone crack face at the end of loading process.

III. PYRAMIDAL IFT METHODS

By virtue of the sharp tip and edges, pyramidal indenters such as Vickers, Berkovich and cube-corner ones are prone to create easy-to-measure radial crack traces (see Fig.4) on the specimen surface. It accounts for the popularity of pyramidal IFT methods in both research and practice. On the other

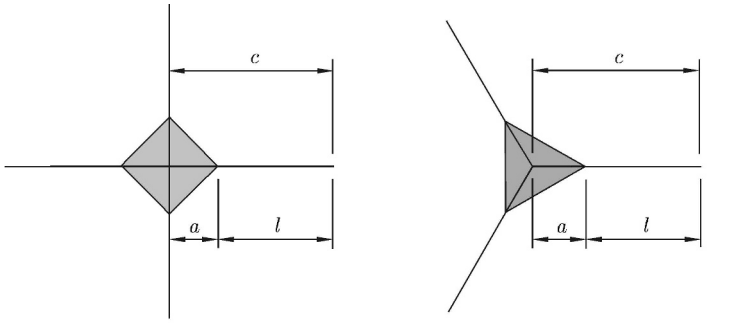

(a) Vickers indenter (b) Berkovich or cube-corner indenter

Fig. 4. Representative dimensions of pyramidal indentation fracture testing methods.

hand, the singularity of stress field under the indenter tip and edges makes it difficult to analytically solve the contact/fracture problems and results in a fact that most existing pyramidal IFT methods were just developed semi-empirically or empirically.

3.1. Theories

3.1.1. Half-penny cracks

As the pioneers attempting to investigate pyramidal indentation fracture problems with an analytical method, in 1976, Evans and Charles[22] proposed a simplified relationship between fracture toughness and measuring parameters for Vickers IFT if radial cracks are well-developed ($c \gg a$). By dimensional analysis and experimental data fitting, they can obtain

$$\frac{K_{\mathrm{IC}}\Phi}{HV\sqrt{a}}\left(\frac{1}{\Phi}\frac{HV}{E}\right)^{2/5} \propto \left(\frac{c}{a}\right)^{-3/2} \tag{1}$$

in which, c is the radial crack size (see Fig.4), a is the half diagonal of the indent, constraint factor $\Phi \approx 3$, HV is Vickers hardness ($HV = F_{\mathrm{m}}/(2a^2)$, where F_{m} is the maximum indentation load), and E is the elastic modulus of the specimen.

In 1980, Lawn et al.[14] advanced Evans and Charles's investigation further by proposing an elastic/plastic indentation fracture model for Vickers IFT. In this model the volume of specimen under indentation is divided into two zones, a semi-spherical plastic zone immediately under the indenter and the surrounding elastic zone outside (see Fig.5). Crack faces below the radial crack traces are assumed as half-penny shape (see Fig.2(d)). The stress field of indentation is treated as the superposition of the reversible part (see Fig.5(b)) caused by pointed indentation load and the irreversible part (see Fig.5(c)) caused by expansion of plastic zone during indentation. In 1982, Yoffe[23] presented an explicit expression for this kind of two-part indentation-induced stress field over the elastic zone. In this model, the circumferential stress at the specimen surface which is responsible for radial cracking can be expressed as

$$\sigma_\theta(r) = -\frac{F\,(1-2\nu)}{2\pi r^2} + \frac{4B\,(1-2\nu)}{r^3} \tag{2}$$

in which, F stands for the indentation load, ν stands for the Poisson's ratio of specimen, and r denotes the polar coordinate which equals to the distance away from the indentation origin. On the right side of Eq.(2), the first term is the reversible part caused by pointed indentation load which will be recovered after withdrawing the indenter, the second term represents the irreversible part caused by expansion of plastic zone during the indentation. B in Eq.(2) is a positive quantity with the dimension of energy ([FL]) which increases during the process of indenter penetrating into specimen and reaches its maximum at the end of loading process, then holds the maximum value all through the unloading phase. Eq.(2) implies that the radial-crack-driving stress increases while F decreases in the unloading phase so that the radial cracks reach their maximum sizes at the end of unloading phase.

If the half-penny cracks are well-developed ($c \gg a$), i.e., the crack fronts extend to the elastic zone, the action of irreversible plastic zone expansion on half-penny crack face after unloading can be

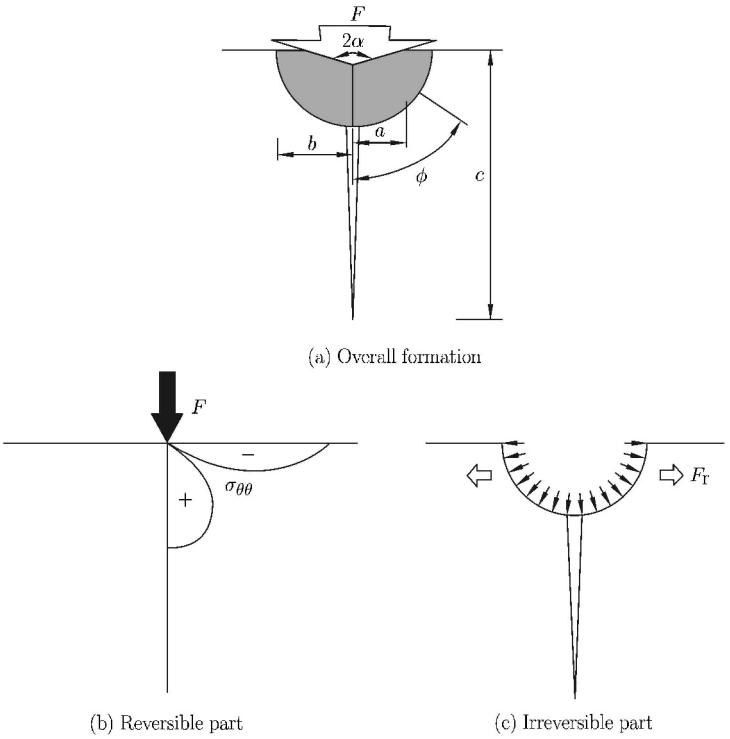

Fig. 5. Schematic of the elastic/plastic indentation fracture model by Lawn et al.[14].

simplified into a pair of opposite centered pointed forces normal to the half-penny cracks[14]:

$$F_{\mathrm{r}} \propto F_{\mathrm{m}} \left(\frac{a}{b}\right) \left(\frac{E}{H}\right) \cot \psi \tag{3}$$

in which, b is the radius of semi-spherical plastic zone, ψ is the face-to-axis angle of the Vickers indenter (74°), H is the Meyer's hardness[24] standing for the contact pressure of indentation. Based on Hill's expanding cavity model[25], Lawn et al.[14] established an approximate relationship between the relative size of plastic zone b/a and E/H as

$$\frac{b}{a} \propto \left(\frac{E}{H}\right)^{1/2} \tag{4}$$

Thus Eq.(3) can be rewritten as

$$F_{\mathrm{r}} \propto F_{\mathrm{m}} \left(\frac{E}{H}\right)^{1/2} (\cot \psi)^{2/3} \tag{5}$$

Using an existing solution[26] of the stress intensity factor for the embedded penny crack subject to a pair of normal pointed forces, the stress intensity factor at front of half-penny crack can be written as

$$K_{\mathrm{r}} \propto f(\phi) \frac{F_{\mathrm{r}}}{c^{3/2}} = f(\phi) \left(\frac{E}{H}\right)^{1/2} (\cot \psi)^{3/2} \frac{F_{\mathrm{m}}}{c^{3/2}} \tag{6}$$

in which, $f(\phi)$ standing for the effect of the specimen surface is an angular function near unity and reaches its maximum at the specimen surface ($\phi = \pi/2$). Thus the fracture toughness should be equal to the stress intensity factor at the half-penny crack front at specimen surface as

$$K_{\mathrm{IC}} = K_{\mathrm{r}}|_{\phi=\pi/2} \tag{7}$$

Combining Eq.(5) with Eq.(4) yields the expression of the fracture toughness as

$$K_{\mathrm{IC}} = \delta \left(\frac{E}{H}\right)^{1/2} \frac{F_{\mathrm{m}}}{c^{3/2}} \tag{8}$$

in which, $\delta \propto f(\pi/2)(\cot\psi)^{3/2}$ is a material-independent constant standing for the influence of indenter geometry and the effect of free specimen surface.

By simplifying Hill's expanding cavity model, Laugier[27] obtained a different approximate relationship between b/a and E/H as

$$\frac{b}{a} \propto \left(\frac{E}{H}\right)^{1/3} \tag{9}$$

and established another expression of fracture toughness for well-developed half-penny cracks induced by Vickers indenter as

$$K_{\mathrm{IC}} = \delta^{\mathrm{L1}} \left(\frac{E}{H}\right)^{2/3} \frac{F_{\mathrm{m}}}{c^{3/2}} \tag{10}$$

3.1.2. Separate radial cracks

In many cases there are well-developed separate radial racks (see Fig.2(b)) instead of coalesced half-penny cracks (see Fig.2(d)) beneath the surface radial crack traces. Based on the existing solution[28] of stress intensity factor for the embedded plane crack subjected to a pair of normal pointed forces, Laugier[13] established the relationship between the stress intensity factors calculated with the assumption of the separate-radial-cracking pattern (K^{R}) and half-penny-cracking pattern (K^{HP}) as follows:

$$K^{\mathrm{R}} = 2\left(\frac{\pi}{\pi+2}\right)^{1/2} \left(\frac{a}{l}\right)^{1/2} K^{\mathrm{HP}} \tag{11}$$

in which, l is the length of the radial crack trace (see Fig.2(a)), thus $c = a+l$. By combining the relationship in Eq.(11) with fracture toughness expression in Eq.(10), Laugier[13] established an expression of fracture toughness for well-developed separate radial cracks produced by Vickers indenter as

$$K_{\mathrm{IC}} = \delta^{\mathrm{L2}} \left(\frac{a}{l}\right)^{1/2} \left(\frac{E}{H}\right)^{2/3} \frac{F_{\mathrm{m}}}{c^{3/2}} \tag{12}$$

in which, δ^{L2} is a material-independent constant.

With the development of instrumented indentation testing (IIT) techniques, the three-sided Berkovich indenter (see Fig.1(b)), which has the same depth-projected area relationship as the four-sided Vickers indenter, becomes the most popular indenter since a three-sided indenter's tip geometry is much easier to be manufactured accurately. Due to their different numbers of edges, when indenting on a brittle specimen, Berkovich and Vickers indenters produce three and four radial cracks, respectively (see Fig.4). Based on Laugier's fracture toughness expression[13] for well-developed separate radial cracks and the relationship between the stress intensity factor and the number of radial cracks proposed by Ouchterlony[29], Dukino and Swain[10] established an expression of fracture toughness for well-developed radial cracks for Berkovich ITF as

$$K_{\mathrm{IC}} = 1.073\delta^{\mathrm{L2}} \left(\frac{a}{l}\right)^{1/2} \left(\frac{E}{H}\right)^{2/3} \frac{F_{\mathrm{m}}}{c^{3/2}} \tag{13}$$

in which, δ^{L2} is the same constant as in Eq.(12). The coefficient 1.073 close to unity implies that difference between Vickers and Berkovich indenters for IFT is not significant.

3.2. Representative Methods

A great number of IFT methods for determining fracture toughness based on the theories mentioned above have been established to date. As for well-developed cracks ($c \gg a$), the methods were mainly established semi-empirically based on the half-penny-cracking models or separate-radial-cracking models introduced in §3.1 and the calibration of test data. As for short radial cracks, also called Palmqvist cracks which do not satisfy the condition of $c \gg a$, the method were generally established empirically based on the calibration of test data.

3.2.1. Well-developed radial cracks

A classic IFT method for well-developed radial cracks using Vickers indenter was established by Anstis et al.[30]. They calibrated the material-independent constant in Eq.(8) on Vickers IFT experimental data on a series of typical brittle materials including glasses and ceramics with known fracture toughness, and obtained $\delta = 0.016 \pm 0.004$[30]. When using this method, Meyer's hardness H is calculated by $H = F_{\rm m}/(2a^2)$, and elastic modulus is usually measured by conventional tensile or bending tests. In this method, 'well-developed' is defined as $c \geq 2a$, which can also act as the common requirement of the relative crack length for other IFT methods utilizing well-developed radial cracks.

By using Anstis et al.'s experimental data[30], Laugier calibrated the material-independent constant in Eq.(10) and obtained $\delta^{\rm L1} = 0.0098 \pm 0.0025$[27] with the assumption of well-developed half-penny cracks, and calibrated the material-independent constant in Eq.(12) and obtained $\delta^{\rm L2} = 0.015 \pm 0.0039$[13] with the assumption of well-developed separate radial cracks.

Pharr et al.[31–33] first utilized the instrumented indentation testing (IIT) techniques (see Appendix in detail) in IFT research. They used Vickers, Berkovich and cube-corner indenters to produce radial cracks, respectively, on a series of typical brittle materials, then used a Berkovich indenter to perform non-cracking IIT on a different area of the specimen surface to measure E and H, and found that Eq.(8) works well for both Vickers and Berkovich indenters if $\delta = 0.016$[31], and works well for cube-corner indenter if $\delta = 0.032 \sim 0.040$[31–33]. They also found that the cube-corner indenter, compared with Vickers and Berkovich indenters, can significantly lower the threshold indentation load for radial cracks initiation due to its much smaller acuity[32].

As for above-mentioned IFT methods even those utilizing IIT techniques, there is a common inconvenience that E or H cannot be measured directly in the IFT. This inconvenience gives rise to the requirement of additional testing and undermines the accuracy of local fracture toughness determination. To solve this problem, Zhang and Feng et al.[34,35] utilized the scaling relationship for pyramidal indention works (see Eq.(39)) to establish a work-based IFT method. Combining Eqs.(8), (37) and (39), given $E_{\rm i} \gg E$ and $\nu = 0.25$ (work for most glasses and ceramics), yields this work-based method's expression:

$$K_{\rm IC} = \lambda \left(\frac{W_{\rm u}}{W_{\rm t}}\right)^{-1/2} \frac{F_{\rm m}}{c^{3/2}} \tag{14}$$

in which, λ is a material-independent constant which is obtained, by calibration with typical brittle materials, 0.0498 for Vickers indenter, and 0.0527 for cube-corner indenter, respectively. All parameters in Eq.(14) can be obtained directly in Vickers or cube-corner IFT because the recovery ratio of indentation work ($W_{\rm u}/W_{\rm t}$) is insensitive to indentation-induced radial cracking[34,35].

There are plenty of other IFT models and methods for well-developed radial cracks in addition to the above mentioned ones, such as Fett et al.'s Vickers IFT methods[36,37] based on opening-profile measurement of radial cracks and Shetty et al.'s wedge-loaded Vickers IFT model[38,39]. Due to their inconvenience or less practice, these models and methods are not discussed in detail in the present paper.

3.2.2. Palmqvist radial cracks

There is no effective analytical model for Palmqvist radial cracks having small values of c/a so far because the plastic zone's action on crack face cannot be simplified into a pair of opposite pointed forces. The existing methods were mainly established empirically.

Based on Evans and Charles's investigation[22], Niihara et ai.[40,41] proposed that different Vickers IFT formulae should be established for well-developed radial cracks ($c \gg a$) and Palmqvist radial cracks (small c/a), respectively. Calibrating on extensive experimental data over Palmqvist range ($0.25 \leq l/a \leq 2.5$) and well-developed range ($c/a \geq 2.5$), Niihara et al.[40] obtained (see Fig.6)

$$\left(\frac{K_{\rm IC}\Phi}{HV\sqrt{a}}\right)\left(\frac{1}{\Phi}\frac{HV}{E}\right)^{2/5} = \begin{cases} 0.035\left(\dfrac{l}{a}\right)^{-1/2} & \left(0.25 \leq \dfrac{l}{a} \leq 2.5\right) \\ 0.129\left(\dfrac{c}{a}\right)^{-3/2} & \left(\dfrac{c}{a} \geq 2.5\right) \end{cases} \tag{15}$$

Lankford[42] found that there exists a common formula for both Palmqvist and well-developed radial cracks if the exponent of c/a is set as -0.156, and obtained a full-range method for Vickers IFT:

$$\left(\frac{K_{\mathrm{IC}}\Phi}{HV\sqrt{a}}\right)\left(\frac{1}{\Phi}\frac{HV}{E}\right)^{2/5}=0.142\left(\frac{c}{a}\right)^{-1.56} \tag{16}$$

Liang et al.[43] empirically established another full-range method for Vickers IFT by taking into account the effect of Poisson's ratio:

$$14\left[1-8\left(\frac{4\nu-0.5}{1+\nu}\right)^4\right]\left(\frac{K_{\mathrm{IC}}\Phi}{HV\sqrt{a}}\right)\left(\frac{1}{\Phi}\frac{HV}{E}\right)^{2/5}=\left(\frac{c}{a}\right)^{c/18a-1.51} \tag{17}$$

which may somewhat lower the uncertainty of fracture toughness determination.

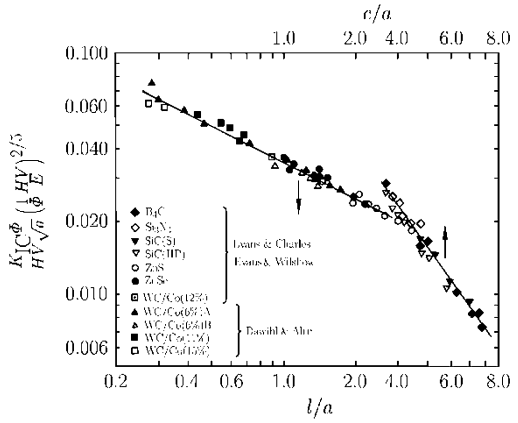

Fig. 6. Calibration of formulae for both well-developed radial cracks Palmqvist radial cracks respectively[40].

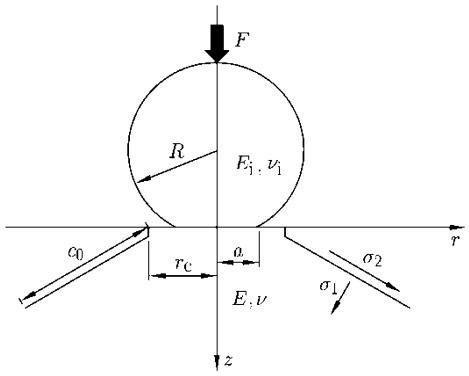

Fig. 7. Schematic of spherical indentation fracture on brittle materials.

IV. SPHERICAL IFT METHODS

Elastic deformation prevails when the spherical indenter is pressed upon brittle materials. The elastic stress field beneath the spherical indenter is non-singular and has been solved analytically[44,45] so that the spherical IFT methods for fracture toughness can be modeled analytically. However, because of the difficulty of accurate measurement of analyzing parameters and the sensitivity to the coefficient of friction and Poisson's ratios, spherical IFT methods are not as popular as Vickers IFT methods in practice.

4.1. Theories

The elastic stress field beneath the spherical indenter can be expressed explicitly in cylindrical coordinates as follows[45]:

$$\begin{aligned}
\frac{\sigma_r}{\sigma_0}&=-\frac{L^3R^2Z}{(L^4+Z^2)(1+L^2)^2}-(1-2\nu)\left[\frac{Z}{L(1+L^2)}\frac{1}{3R^2}\left(1-\frac{Z^3}{L^3}\right)\right]\\
&\quad+\frac{Z}{L}\left[L(1+\nu)\arctan\left(\frac{1}{L}\right)-(1-\nu)\frac{L^2}{1+L^2}-2\nu\right]\\
\frac{\sigma_\theta}{\sigma_0}&=-\frac{1-2\nu}{3R^2}\left(1-\frac{Z^3}{L^3}\right)+\frac{Z}{L}\left[L(1+\nu)\arctan\left(\frac{1}{L}\right)-(1-\nu)\frac{L^2}{1+L^2}-2\nu\right]\\
\frac{\sigma_z}{\sigma_0}&=-\frac{Z^3}{L(L^4+Z^2)}\\
\frac{\tau_{zr}}{\sigma_0}&=-\frac{LRZ^2}{(L^4+Z^2)(1+L^2)}\\
\frac{\tau_{r\theta}}{\sigma_0}&=\frac{\tau_{z\theta}}{\sigma_0}=0
\end{aligned} \tag{18}$$

in which, $\sigma_0 = 3F/(2\pi a^2)$, L is

$$L = \sqrt{\frac{1}{2}\left[R^2 + Z^2 - 1 + \sqrt{(R^2 + Z^2 - 1)^2 + 4Z^2}\right]} \tag{19}$$

and $R^2 = X^2 + Y^2$, $X = x/a$, $Y = y/a$, $Z = z/a$ are normalized coordinates, a is the radius of contact area (see Fig.7) and can be calculated by

$$a^3 = \frac{4kFR}{3E} \tag{20}$$

where k can be expressed as

$$k = \frac{9}{16}\left[(1 - \nu_{\rm i}^2) + (1 - \nu^2)\frac{E}{E_{\rm i}}\right] \tag{21}$$

in which, $\nu_{\rm i}$ and $E_{\rm i}$ stand for the Poisson's ratio and elastic modulus of the indenter, respectively.

From Eq.(18), the first principal stress can be obtained as

$$\sigma_1 = \frac{\sigma_r + \sigma_z}{2} + \sqrt{\left(\frac{\sigma_r - \sigma_z}{2}\right)^2 + \tau_{zr}^2} \tag{22}$$

in the direction of

$$\tan(2\alpha) = \frac{2\tau_{zr}}{\sigma_z - \sigma_r} \tag{23}$$

The cone crack is driven by σ_1, thus the stress intensity factor at the front of cone crack can be calculated by integration over the cone crack length, as[18,19,45,46]

$$K_{\rm I} = 2\left(\frac{c_0}{\pi}\right)^{1/2}\int_0^{c_0}\frac{\sigma_1(c)}{(c_0^2 - c^2)^{1/2}}{\rm d}c \tag{24}$$

Warren[21] considered the superficial ring crack rather than the deeply located cone crack. The stress intensity factor $K_{\rm I}$ at a pre-existing ring defect can be expressed as

$$\frac{K_{\rm I}}{p_0\sqrt{\pi a}} = \mu\sqrt{\frac{c_{\rm ring}}{a}} \tag{25}$$

where p_0 denotes the peak pressure over the contact area and can be expressed as

$$p_0 = \frac{3F}{2\pi a^2} \tag{26}$$

In Eq.(25), $c_{\rm ring}$ denotes the size (viz. depth) of the ring defect, μ is a dimensionless function as

$$\mu = f\left(\frac{r}{a}, \frac{c_{\rm ring}}{a}, \nu\right) \tag{27}$$

Considering the condition that the ring defect extends forward at a threshold indentation load, $F = F^*$, one can obtain fracture toughness $K_{\rm IC}$ by inserting Eqs.(21), (22), (26) and (37) into Eq.(25), i.e.,

$$\frac{E_{\rm r}F^*}{RK_{\rm IC}^2} = \frac{\pi}{3\mu^2(c_{\rm ring}/a)} \tag{28}$$

in which, $E_{\rm r}$ is the reduced modulus which can be calculated using Eq.(37).

4.2. Representative Methods

Frank and Lawn and Zeng et al.[18,19,45,46] proposed an spherical IFT method based on Eq.(24). In this method, fracture toughness can be obtained by equaling its value to the stress intensity factor at the cone crack front at the end of loading process, i.e.,

$$K_{\rm IC} = 2\left(\frac{c_0}{\pi}\right)^{1/2}\int_0^{c_0}\frac{\sigma_1(c)}{(c_0^2 - c^2)^{1/2}}{\rm d}c \tag{29}$$

This method is just applicable to transparent materials because the size of cone crack c_0 (see Fig.7) should be measured to calculate the fracture toughness and cross-sectioning specimens may arise dramatic re-extension of cone crack and yields the unacceptable c_0 measurement[47].

Warren[21] proposed a spherical IFT method applicable to both transparent and opaque materials which utilizes ring cracks. Warren conducted numerical investigation on Eq.(28), and found the relationship between $K_{\rm IC}$ and the minimum F^*, viz. $F_{\rm C}$ as

$$K_{\rm IC} = \left(\frac{E_{\rm r} F_{\rm C}}{\xi R}\right)^{1/2} \tag{30}$$

in which ξ is a dimensionless constant dependent on the Poisson's ratio[21]. $F_{\rm C}$ is usually detected using an acoustic emission (AE) detector. It should be noted that it is not easy to distinguish between the AE signals associated with indentation cracking and those associated with other potential sources such as friction between the indenter and the specimen[48].

V. DISCUSSION

5.1. Pyramidal IFT Methods versus Spherical IFT Methods

According to the above investigation on the developing state of IFT methods using pyramidal indenters and spherical indenters so far, it is found that pyramidal IFT methods can serve broader categories of brittle materials since no transparent feature are needed and the characteristic parameters can be easily and accurately measured. Existing pyramidal IFT methods were developed semi-empirically or empirically and resulted in the variety of formulae of methods. As for the spherical IFT methods based on analytical models, the working range is narrow or the precise measurement is difficult.

Therefore the pyramidal IFT methods should be preferred in the practice of measuring fracture toughness. However, the spherical IFT also can play an important role in theoretical analysis of fracture phenomena other than probing toughness.

5.2. Sources of the Diversity of Pyramidal IFT Methods

The diversity of pyramidal IFT methods are mainly caused by three factors: (i) Different cracking features such as well-developed radial cracks and Palmqvist radial cracks. (ii) Mathematical difficulties, which resulted in plenty of approximate solutions to a same problem. For example, the relationship between b/a and E/H should be established by solving the equation[25]

$$\frac{E}{H} = \frac{9\left[(1-\nu)\,\beta^3 - 2\,(1-2\nu)/3\right]}{2\,(1+\ln\beta^3)} \tag{31}$$

in which, $\beta = b/r_0 \propto b/a$ is the relative size of plastic zone for indentations using a pyramidal indenter. It is difficult to obtain β's rigorous solution from Eq.(31). Different approximate solutions of β by researchers result in the variety of the exponent of E/H in formulae of different existing pyramidal IFT methods. (iii) Different coverage of reference materials selected for calibrating formulae of pyramidal IFT methods.

5.3. Considerations in Choosing IFT Methods and Indenter Geometries

Due to the diversity of pyramidal IFT methods, cautions should be taken when choosing the appropriate method for a certain case. The following factors should be considered when choosing methods: (i) geometric features of specimen. For example, cube-corner indenter is preferred for much smaller specimens and films. (ii) Features of the cracking pattern. A method based on similar assumption of cracking pattern of the test material should be adopted. (iii) Coverage of the reference materials. A method whose reference materials for formula calibration cover the type of the test material should be preferred.

5.4. Gap Between Existing IFT Methods and Standardization

Compared with those standardized conventional fracture testing (CFT) methods, existing indentation fracture testing (IFT) methods have two crucial unsolved problems which accounts for the criticism[49] and shape the gap between the existing IFT methods and standardization. The first problem is the

diversity of existing IFT methods which were mainly caused by non-analytical solution to the half-space contact/fracture problem, especially for pyramidal IFT methods. The second one is indefinite working range of certain IFT methods. Future developments in analytically modeling of half-space sharp contact/fracture problems and extensive experimental investigation on the working range of IFT methods will increase their acceptance in practice and reach the requirements of standardization.

VI. CONCLUSION

Indentation fracture testing is a convenient, sometimes exclusive tool, to probe fracture toughness of brittle materials on small scales since it can avoid the size and shape limits on specimens required in standardized conventional fracture testing. The past half century has seen the substantial development on the investigation of cracking patterns and the establishment of testing methods for both pyramidal and spherical indentation fracture testing. Considering the immaturity and diversity of current indentation fracture testing, cautions and expertise should be taken while using indentation fracture testing methods to probe fracture toughness of brittle materials. Future development in analytical solution to half-space sharp contact/fracture problems and extensive investigation on working range of existing methods are in demand to increase the acceptance of indentation fracture testing in practice and realize the standardization.

References

[1] Palmqvist,S., A method to determine the toughness of brittle materials, especially hard metals. *Jerkontorets Ann.*, 1957, 141: 303-307.

[2] Palmqvist,S., The work for the formation of a crack during Vickers indentation as a measure of the toughness of hard metals. *Arch. Einsenhuttenwes*, 1962, 33: 629-634.

[3] Palmqvist,S., The work for the formation of a crack as a measure of hard metals. *Jernkontorets Ann.*, 1963, 147: 107-110.

[4] Cook,R.F. and Pharr,G.M., Direct observation and analysis of indentation cracking in glasses and ceramics. *Journal of The American Ceramic Society*, 1990, 73(4): 787-817.

[5] Ostojic,P. and McPherson,R., A review of indentation fracture theory: Its development, principles and limitations. *International Journal of Fracture*, 1987, 33(4): 297-312.

[6] Ponton,C.B. and Rawlings,R.D., Vickers indentation fracture toughness test part 1 review of literature and formulation of standardised indentation toughness equations. *Materials Science And Technology*, 1989, 5(9): 865-872.

[7] Ponton,C.B. and Rawlings,R.D., Vickers indentation fracture toughness test—Part 2: Application and critical evaluation of standardised indentation toughness equations. *Materials Science And Technology*, 1989, 5(10): 961-976.

[8] Chen,J.J., Indentation-based methods to assess fracture toughness for thin coatings. *Journal of Physics D-Applied Physics*, 2012, 45: 203001.

[9] ISO14577:2002, Metallic materials — instrumented indentation test for hardness and materials parameters. International Organization for Standardization, Geneva, Switzerland.

[10] Dukino,R.D. and Swain,M.V., Comparative measurement of indentation fracture toughness with Berkovich and Vickers indenters. *Journal of the American Ceramic Society*, 1992, 75(12): 3299-3304.

[11] Tandon,R., A technique for measuring stresses in small spatial regions using cube-corner indentation: application to tempered glass plates. *Journal of The European Ceramic Society*, 2007, 27(6): 2407-2414.

[12] Schiffmann,K.I., Determination of fracture toughness of bulk materials and thin films by nanoindentation: comparison of different models. *Philosophical Magazine*, 2011, 91(7-9): 1163-1178.

[13] Laugier,M.T., New formula for indentation toughness in ceramics. *Journal of Materials Science Letters*, 1987, 6(3): 355-356.

[14] Lawn,B.R., Evans,A.G. and Marshall,D.B., Elastic/plastic indentation damage in ceramics: the median/radial crack system. *Journal of The American Ceramic Society*, 1980, 63(9-10): 574-581.

[15] Marshall,D.B. and Lawn,B.R., Residual-stress effects in sharp contact cracking—1. Indentation fracture mechanics. *Journal of Materials Science*, 1979, 14(8): 2001-2012.

[16] Morris,D.J. and Cook,R.F., In situ cube-corner indentation of soda-lime glass and fused silica. *Journal of The American Ceramic Society*, 2004, 87(8): 1494-1501.

[17] Roesler,F.C., Brittle fractures near equilibrium. *Proceedings of the Physical Society, Section B*, 1956, 69(10): 981-992.

[18] Frank,F.C. and Lawn,B.R., On the theory of Hertzian fracture. *Proceedings of the Royal Society of London. Series A, Mathematical and Physical Sciences*, 1967, 299: 291-306.

[19] Zeng,K., Breder,K. and Rowcliffe,D.J., The Hertzian stress field and formation of cone cracks—ii. determination of fracture toughness. *Acta Metallurgica et Materialia*, 1992, 40(10): 2601-2605.
[20] Zeng,K., Breder,K., Rowcliffe,D.J. and Herrström,C., Elastic modulus determined by Hertzian indentation. *Journal of Materials Science*, 1992, 27(14): 3789-3792.
[21] Warren,P.D., Determining the fracture toughness of brittle materials by Hertzian indentation. *Journal Of The European Ceramic Society*, 1995, 15(3): 201-207.
[22] Evans,A.G. and Charles,E.A., Fracture toughness determinations by indentation. *Journal of The American Ceramic Society*, 1976, 59(7-8): 371-372.
[23] Yoffe,E., Elastic stress fields caused by indenting brittle materials. *Philosophical Magazine, A*, 1982, 46(4): 617-628.
[24] Tabor,D., The Hardness of Metals. London, UK: Oxford University Press, 1951.
[25] Hill,R., The Mathematical Theory of Plasticity. New York, USA: Oxford University Press, 1998.
[26] Rooke,D.P. and Cartwright,D.J., Compendium of Stress Intensity Factors. London: Her Majesty's Stationery Office, 1975.
[27] Laugier,M.T., The elastic/plastic indentation of ceramics. *Journal of Materials Science Letters*, 1985, 4(12): 1539-1541.
[28] Oore,M. and Burns,D.J., Estimation of stress intensity factors for embedded irregular cracks subjected to arbitrary normal stress fields. *Journal of Pressure Vessel Technology*, 1980, 102(2): 202-211.
[29] Ouchterlony,F., Stress intensity factors for the expansion loaded star crack. *Engineering Fracture Mechanics*, 1976, 8(2): 447-448.
[30] Anstis,G.R., Chantikul,P., Lawn,B.R. and Marshall,D.B., A critical evaluation of indentation techniques for measuring fracture toughness—I. Direct crack measurements. *Journal of the American Ceramic Society*, 1981, 64(9): 533-538.
[31] Pharr,G.M., Harding,D.S. and Oliver,W.C., Measurement of fracture toughness in thin films and small volumes using nanoindentation methods. In: Mechanical Properties and Deformation Behavior of Materials Having Ultra-fine Microstructures, Edited by Nastasi,M., Parkin,D.M. and Gleiter,H., Kluwer Academic Publishers, Dordrecht, the Netherlands, 1993: 449-461.
[32] Harding,D.S., Oliver,W.C. and Pharr,G.M., Cracking during nanoindentation and its use in the measurement of fracture toughness. *Materials Research Society Symposium Proceedings*, 1995, 356: 663-668.
[33] Pharr,G.M., Measurement of mechanical properties by ultra-low load indentation. *Materials Science and Engineering A*, 1998, 253(1-2): 151-159.
[34] Zhang,T.H., Feng,Y.H., Yang,R. and Jiang,P., A method to determine fracture toughness using cube-corner indentation. *Scripta Materialia*, 2010, 62(4): 199-201.
[35] Feng,Y.H., Zhang,T.H. and Yang,R., A work approach to determine Vickers indentation fracture toughness. *Journal of The American Ceramic Society*, 2011, 94(2): 332-335.
[36] Fett,T., Computation of the crack opening displacements for Vickers indentation cracks. Report FZKA 6757, Forschungszentrum Karlsruhe, Karlsruhe, Germany, 2002.
[37] Fett,T., Kounga,A.B. and Rödel,J., Stresses and stress intensity factor from cod of Vickers indentation cracks. *Journal of Materials Science*, 2004, 39(6): 2219-2221.
[38] Shetty,D.K., Rosenfield,A.R. and Duckworth,W., Analysis of indentation crack as a wedge-loaded half-penny crack. *Journal of The American Ceramic Society*, 1985, 68(2): C65-C67.
[39] Shetty,D.K., Wright,I.G., Mincer,P.N. and Clauer,A.H., Indentation fracture of wc-co cermets. *Journal of Materials Science*, 1985, 20(5): 1873-1882.
[40] Niihara,K., Morena,R. and Hasselman,D.P.H., Evaluation of K_{IC} of brittle solids by the indentation method with low crack-to-indent ratios. *Journal of Materials Science Letters*, 1982, 1(1): 13-16.
[41] Niihara,K., A fracture mechanics analysis of indentation-induced Palmqvist crack in ceramics. *Journal of Materials Science Letters*, 1983, 2(5): 221-223.
[42] Lankford,J., Indentation microfracture in the Palmqvist crack regime: implications for fracture toughness evaluation by the indentation method. *Journal of Materials Science Letters*, 1982, 1(11): 493-495.
[43] Liang,K.M., Orange,G. and Fantozzi,G., Evaluation by indentation of fracture toughness of ceramic materials. *Journal of Materials Science*, 1990, 25(1): 207-214.
[44] Johnson,K.L., Contact Mechanics. Cambridge, UK: Cambridge University Press, 1985.
[45] Zeng,K., Breder,K. and Rowcliffe,D.J., The Hertzian stress field and formation of cone cracks—I. Theoretical approach. *Acta Metallurgica et Materialia*, 1992, 40(10): 2595-2600.
[46] Lawn,B.R., Hertzian fracture in single crystals with the diamond structure. *Journal of Applied Physics*, 1968, 39(10): 4828-4836.
[47] Geandier,G., Denis,S. and Mocellin,A., Float glass fracture toughness determination by Hertzian, contact: experiments and analysis. *Journal of Non-crystalline Solids*, 2003, 318(3): 284-295.

[48] Faisal,N.H., Ahmed,R. and Reuben,R.L., Indentation testing and its acoustic emission response: applications and emerging trends. *International Materials Reviews*, 2011, 56(2): 98-142.
[49] Quinn,G.D. and Bradt,R.C., On the Vickers indentation fracture toughness test. *Journal of The American Ceramic Society*, 2007, 90(3): 673-680.
[50] Oliver,W.C. and Pharr,G.M., Improved technique for determining hardness and elastic modulus using load and displacement sensing indentation experiments. *Journal of Materials Research*, 1992, 7(6): 1564-1583.
[51] King,R.B., Elastic analysis of some punch problems for a layered medium. *International Journal of Solids And Structures*, 1987, 23(12): 1657-1664.
[52] Cheng,Y.T. and Cheng,C.M., Relationships between hardness, elastic modulus, and the work of indentation. *Applied Physics Letters*, 1998, 73(5): 614-616.
[53] Yang,R., Zhang,T.H., Jiang,P. and Bai,Y.L., Experimental verification and theoretical analysis of the relationships between hardness, elastic modulus, and the work of indentation. *Applied Physics Letters*, 2008, 92(23): 231906.
[54] Yang,R., Zhang,T.H. and Feng,Y.H., Theoretical analysis of the relationships between hardness, elastic modulus, and the work of indentation for work-hardening materials. *Journal of Materials Research*, 2010, 25(11): 2072-2077.

APPENDIX

Common instrumented indentation testing techniques

Instrumented indentation testing (IIT) techniques are mainly aimed to probe mechanical parameters and properties of specimens at small scales. The basic work flow of IIT techniques is to push an indenter into a flat sample surface and withdraw it, then to analyze the load-depth (F-h) curve to obtain mechanical parameters and properties. IIT techniques have played an important role in the development of indentation fracture testing (IFT) methods in the past twenty years. In this section, some commonly accepted IIT techniques which have facilitated IFT development are to be introduced. The IIT methods for determining H and E have been standardized[9,50].

The unloading curve can be described using a power-law function

$$F = B\left(h - h_{\mathrm{f}}\right)^{m} \tag{32}$$

With the least square fitting on the unloading curve, one can obtain B, h_{f} and m. Then the contact stiffness S at the initiation of unloading can be obtained by calculating the slope of unloading curve at the maximum indentation depth h_{m}:

$$S = \left.\frac{\mathrm{d}F}{\mathrm{d}h}\right|_{h=h_{\mathrm{m}}} = Bm\left(h_{\mathrm{m}} - h_{\mathrm{f}}\right)^{m-1} \tag{33}$$

The contact depth h_{c} can be calculated using

$$h_{\mathrm{c}} = h_{\mathrm{m}} - \varepsilon\frac{F_{\mathrm{m}}}{S} \tag{34}$$

where ε is constant, 0.75. The projected contact area can be determined by area function

$$A\left(h_{\mathrm{c}}\right) = \sum_{i=0}^{8} C_i h_{\mathrm{c}}^{1/2^{i-1}} \tag{35}$$

This area function should be calibrated beforehand and regularly on standard reference block with known elastic modulus. According to ISO14577[9], if indentation depth is beyond 6 μm, area function can be calculated using the depth-projected area correlation of the ideal pyramidal indenter geometry, for example, $A(h_{\mathrm{c}}) = 24.5h_{\mathrm{c}}^2$ for Vickers indenter and Berkovich indenter, and $A(h_{\mathrm{c}}) = 2.60h_{\mathrm{c}}^2$ for cube-corner indenter. The reduced modulus can be obtained by

$$E_{\mathrm{r}} = \frac{\sqrt{\pi}}{2\beta}\frac{S}{\sqrt{A}} \tag{36}$$

in which, β is a constant just depending on the indenter geometry, where $\beta = 1.034$ for Berkovich indenter and cube-corner indenter, and $\beta = 1.012$ for Vickers indenter[51]. Then the elastic modulus can be calculated by

$$\frac{1}{E_{\mathrm{r}}} = \frac{1-\nu_{\mathrm{i}}^2}{E_{\mathrm{i}}} + \frac{1-\nu^2}{E} \tag{37}$$

in which $\nu_{\rm i}$ and $E_{\rm i}$ are the Poisson's ratio and elastic modulus of the indenter. The hardness can be calculated by dividing the indentation load by the projected contact area as

$$H = \frac{F_{\rm m}}{A\left(h_{\rm c}\right)} \tag{38}$$

It should be noted, from Eq.(34), that sink-in ($h_{\rm c} < h$, see Fig.8) feature is assumed in IIT techniques for determining E and H. Thus there may be significant error in the measurements of E and H for indentations with a pile-up ($h_{\rm c} > h$) phenomenon.

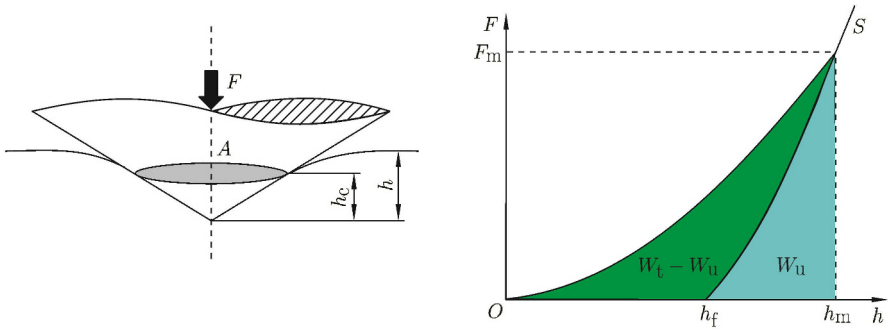

(a) Geometric parameters (b) Load-depth parameters

Fig. 8. Schematic of instrumented indentation testing.

There is an important relationship for indentations using geometrically self-similar indenters such as pyramidal ones including Vickers, Berkovich and cube-corner indenters, as

$$\frac{H}{E_{\rm r}} \approx \kappa \frac{W_{\rm u}}{W_{\rm t}} \tag{39}$$

in which, the total loading work $W_{\rm u} = \int_0^{h_{\rm m}} F_{\rm unloading}(h){\rm d}h$ represents the area under the loading part of F-h curve (see Fig.8), the unloading work $W_{\rm t} = \int_0^{h_{\rm m}} F_{\rm loading}(h){\rm d}h$ represents the area under the unloading part of F-h curve (see Fig.8), and κ is a constant depending on the indenter's tip included angle[52–54]. A great advantage of the relationship revealed in Eq.(39) is that it works for both sink-in and pile-up indentations.